Ceramics International 44 (2018) 7917–7925

Contents lists available at ScienceDirect

Ceramics International

journal homepage: www.elsevier.com/locate/ceramint

Characterization of luminescent $SrAl_2O_4$ films doped with terbium and europium ions deposited by ultrasonic spray pyrolysis technique

R.M. Calderón-Olvera[a,b], E.A. Albanés-Ojeda[a,b], M. García-Hipólito[b,*], J.M. Hernández-Alcántara[c], M.A. Álvarez-Perez[d], C. Falcony[e], O. Álvarez-Fregoso[b]

[a] Posgrado en Ciencias e Ingeniería de Materiales, UNAM, apartado postal 70-360, Coyoacán 04510, CDMX, Mexico
[b] Departamento de Materiales Metálicos y Cerámicos, Instituto de Investigaciones en Materiales, Universidad Nacional Autónoma de México, UNAM, apartado postal 70-360, Coyoacán 04510, CDMX, Mexico
[c] Instituto de Física, Universidad Nacional Autónoma de México, UNAM, apartado postal 70-360, Coyoacán 04510, CDMX, Mexico
[d] Laboratorio de Bioingeniería de Tejidos; DEPeI, Facultad de Odontología, UNAM, Circuito Exterior s/n. Cd. Universitaria, 04510 Coyoacán, CDMX, Mexico
[e] Departamento de Física, CINVESTAV-IPN, apartado postal 14-740, 07000 México, D.F., Mexico

ARTICLE INFO

Keywords:
Luminescence
Films
$SrAl_2O_4:Tb^{3+}$: Eu^{3+}
Spray pyrolysis

ABSTRACT

$SrAl_2O_4$, $SrAl_2O_4:Tb^{3+}$ and $SrAl_2O_4:Eu^{3+}:Eu^{2+}$ films were synthesized by means of the ultrasonic spray pyrolysis technique. These samples, characterized by X-Ray Diffraction, showed the monoclinic phase of the strontium aluminate. Images of the surface morphology of these films were obtained by SEM and the chemical composition was measured by EDS and XPS. The photoluminescence and cathodoluminescence characteristics of the films were studied as a function of the terbium and europium concentrations. The optimal PL emission intensities were reached at 8 at% for terbium doped films and 6 at% for europium doped samples. The CL emission spectra for europium doped films showed the typical bands of Eu^{3+} ions and also a broadband centered at 525 nm which is attributed to Eu^{2+} ions. XPS measurements confirm the presence of Eu^{3+} and Eu^{2+} in europium doped $SrAl_2O_4$ films, without having been subjected to a reducing atmosphere. Chromatic diagrams exhibited green color for $SrAl_2O_4:Tb^{3+}$ films, red and yellow colors for $SrAl_2O_4:Eu^{3+}:Eu^{2+}$ films. The PL decay curves were also obtained: the averaged decay time was 2.7 ms for $SrAl_2O_4:Tb^{3+}$ films and 1.9 ms for $SrAl_2O_4:Eu^{3+}$ films. Similar results were obtained by the stretched exponential model.

1. Introduction

The aluminates of the alkaline earths (Be, Mg, Ca, Sr, Ba and Ra) doped with Eu^{2+} have been studied since the late 1960's [1,2]. Matsuzawa et al. showed that $SrAl_2O_4$ doped with Eu^{2+} and Dy^{3+} contains long-lasting phosphorescent properties [3] much better than ZnS:Cu [4]. $SrAl_2O_4$ is considered a good luminescent material with high brightness, a great chemical stability [5,6] and has a wide bang gap (6.5 eV) [7]. This material has been used in infinity of investigations in the last four decades and is currently being studied for possible applications in electronic devices. Some of the applications of $SrAl_2O_4$ that have been made so far include: thermoluminescence [8–11] optical fiber [12–15] forensic medicine [16,17] tissue regeneration [18] and for UV LED's [19,20], among many others.

Rare earth ions (RE) are widely used for doping in ceramic materials, due to their optical properties that characterize the lanthanide elements [21]; when these elements are introduced in materials such as $SrAl_2O_4$ they give rise to remarkable luminescent properties. As a consequence, $SrAl_2O_4$: RE is a material widely used in new long-lasting (phosphorescent) luminescent materials. The strontium aluminate has been studied in several contributions in the powders form synthesized by the following techniques: sol-gel [22–25], solid-state reaction [26–28], combustion synthesis [29,30] and co-precipitation [31]. But, there are relatively few publications about $SrAl_2O_4$ in films form and the most used deposition techniques include: sputtering [32,33], ion-beam evaporation [34] and pulsed laser deposition (PLD) [35–38]; which are relatively expensive techniques because they use costly vacuum systems. The ultrasonic spray pyrolysis technique is a simple process to synthesis powders and thick and thin films which is suitable for industrial applications since it does not require expensive vacuum systems; this generates a less cost of the produced materials.

The main contribution of this research is the successful deposition of $SrAl_2O_4$, $SrAl_2O_4:Eu^{3+}:Tb^{3+}$ films by the relatively simple and economical ultrasonic spray pyrolysis technique; in addition, doping with terbium and europium has generated the emission of several colors: green, red and yellow. Unexpectedly the cathodoluminescence spectra

* Corresponding author.
E-mail address: maga@unam.mx (M. García-Hipólito).

https://doi.org/10.1016/j.ceramint.2018.01.229
Received 6 October 2017; Received in revised form 26 January 2018; Accepted 27 January 2018
Available online 31 January 2018

revealed the presence of bands corresponding to the Eu^{2+} ions (green emissions). To our best knowledge, a study like this has not been published in the literature of the subject.

2. Experimental details

The ultrasonic spray pyrolysis technique consists in generating an aerosol by an ultrasonic atomizer from a precursor solution; this aerosol is transported by means of a carrier gas to the substrate (previously heated) where the film grows. In this case, the precursor solution for the deposition of $SrAl_2O_4$, $SrAl_2O_4$:Tb^{3+} and $SrAl_2O_4$:Eu^{3+}:Eu^{2+} films consisted of: Aluminum trichloride hexahydrate (99% purity), Strontium dichloride hexahydrate (99% purity) meantime, the incorporation of terbium ions was reached using Terbium trichloride hexahydrate (99.99% purity) and the source of europium was Europium trichloride hexahydrate (99.99% purity). All precursors were dissolved in de-ionized water (18 MΩ cm). The chemical reagents come from Sigma-Aldrich Chemical Co. The molarity of these solutions was 0.07 M. Filtered air at a rate of 10 l/minute was used as carrier gas; doping concentrations of the luminescent activators (terbium and europium) were varied as follows: 0, 2, 4, 6, 8 and 10 at% (atomic percent). All films were deposited a 550 °C during 10 min on quartz substrates (1 × 1.5 cm^2) and annealed at 800 °C (16 h) in a normal atmosphere in a laboratory oven.

The crystalline features of the films were observed by X-Ray Diffraction (XRD) with a diffractometer (Ultima IV Rigaku) using radiation from CuKα (λ = 1.5406 Å) with 40 kV/44 mA. The surface morphology of the samples was analyzed by a scanning electron microscope (SEM) Jeol Scanning Electron Microscope model JSM-7600F with a voltage of 0.50 kV. The chemical composition of the films was measured by EDS (Electron Dispersive Spectroscopy) in the above-mentioned SEM equipment. XPS measurements were carried out using a system of ultra-high evacuation (UHV) of Physical Electronic, Scanning XPS Microprobe PHI 5000 Versa-Probe II with an erosion time of 10 min per sample. Photoluminescence (PL) spectra (excitation-emission) and decay time measurements were obtained by means of a spectrofluorometer Fluoro-Max-P from JobinYvon Horiba. The cathodoluminescence (CL) measurements were carried out by means of a Luminoscope model ELM-2 MCA, RELION Co., which has a vacuum chamber where the samples are positioned with an approximate pressure of 10^{-3} Torr. The electron beam current was 0.3 mA with variations in the accelerating voltages ranging from 5 to 12 kV, the electron beam was deflected through a 90° angle to bombard the films normal to the surface. The emitted light from the films was collected by an optical fiber bundle and fed into the above-cited spectrofluorometer.

3. Results and discussions

Fig. 1 shows diffractograms of $SrAl_2O_4$, $SrAl_2O_4$:Tb^{3+} (8 at%) and $SrAl_2O_4$:Eu^{3+} (6 at%) films deposited at 550 °C and annealed at 800 °C; Fig. 1(a), (b) and (c), respectively. In all cases appears peaks which correspond to the monoclinic phase of $SrAl_2O_4$ with a 2P1 space group, according to JCPDS no. 01-074-0794. Fig. 1(d) shows the diffractogram for a $SrAl_2O_4$ film deposited to 550 °C without annealing, it is possible to observe an absence of the diffraction peaks. The most notable peaks are centered in 2Θ = 20.30°, 29.39° and 35.19° followed by peaks with lower intensity in 28.53° and 30.0°. The Miller indices corresponding to the three most intense peaks are: (−111), (220) and (031) respectively, while the indices belonging to the lower intensity peaks are: (−211) and (211), respectively. The lattice parameters of the monoclinic phase are a = 8.447 Å, b = 8.816 Å, c = 5.163 Å and β = 93.42. The crystal size was estimated by means of the Scherer formula, taking the three films with the most intense bands in $2\Theta_1$ = 20.30°, $2\Theta_2$ = 29.39° and $2\Theta_3$ = 35.19°. The obtained values were: 24.4 nm for $SrAl_2O_4$, 26.39 nm for $SrAl_2O_4$:Tb^{3+} and 27.82 nm for $SrAl_2O_4$:Eu^{3+}. In this case, it is observed that as the TR (terbium and europium) impurities

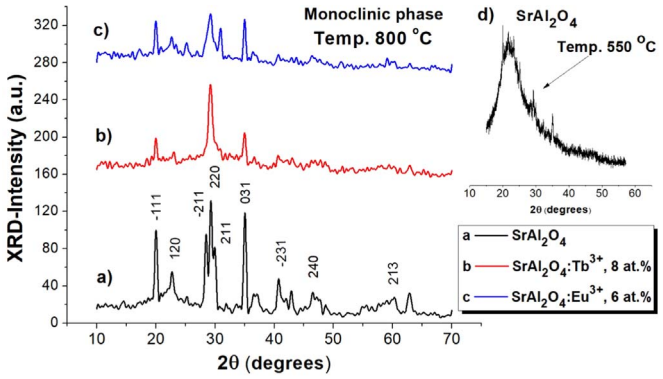

Fig. 1. XRD diffractograms of a) $SrAl_2O_4$, b) $SrAl_2O_4$:Tb^{3+} (8 at%) and c) $SrAl_2O_4$:Eu^{3+} (6 word at%) films deposited at 550 °C and annealed at 800 °C; d) $SrAl_2O_4$ film deposited at 550 °C without annealing.

are incorporated into the host lattice the diffraction peaks decrease in intensity. Most likely this is because the presence of terbium and europium ions distorts to some extent the host lattice and that causes a loss of crystalline quality. However, even with the presence of the impurities, the main peaks of the monoclinic phase of $SrAl_2O_4$ are clearly observed.

Table 1 shows the atomic percentages of oxygen, aluminum, strontium and terbium inside the $SrAl_2O_4$:Tb^{3+} films as a function of the doping concentration as measured by EDS. These films were deposited at 550 °C and annealed at 800 °C. As expected the amounts of terbium rises as the doping concentration increases. The atomic concentrations of oxygen and strontium remain close to their ideal value and the atomic content of aluminum is below of its stoichiometric value; this fact suggests the possibility that terbium ions are introduced into sites of aluminum ions in the $SrAl_2O_4$ host lattice. For the moment, we have no experiments to support this suggestion, so this possibility is merely speculative.

Table 2 presents the atomic percentages of oxygen, aluminum, strontium and europium inside the $SrAl_2O_4$:Eu^{3+} films as a function of the doping concentration as measured by EDS. In this case, the concentrations of oxygen and strontium are close to their ideal values. The concentration of aluminum is below its ideal value and obviously, the concentration of europium ions increases with the increase of the doping concentration.

Fig. 2 shows SEM micrographs of the surface morphology for $SrAl_2O_4$, $SrAl_2O_4$:Tb^{3+} and $SrAl_2O_4$:Eu^{3+} films deposited at 550 °C and annealed at 800 °C. In all cases, very rough surfaces formed by clusters of spheroidal particles are observed. Rough surfaces are typical of films deposited by the ultrasonic spray pyrolysis technique when inorganic reagents (dissolved in water) are used as the precursor solution. From the micrographs, it is seen that the incorporation of the activators of the luminescence (terbium and europium) have an effect on the characteristics of the surface morphology of the analyzed films. The diameters of spheroidal particles in $SrAl_2O_4$ films are about 1.5–2 μm,

Table 1
Atomic percent of the oxygen, aluminum, strontium and terbium as measured by EDS for different concentrations of terbium ions inside the $SrAl_2O_4$:Tb^{3+} films.

Atomic % ± 0.5%				
At%	**O**	**Al**	**Sr**	**Tb**
Tb 0	56.0	31.0	13.0	0
Tb 2	64.0	21.0	14.0	1.0
Tb 4	59.0	25.0	15.0	1.0
Tb 6	59.0	23.0	16.0	2.0
Tb 8	57.0	24.0	16.0	3.0
Tb 10	55.0	27.0	15.0	3.0

Table 2
Atomic percent of the oxygen, aluminum, strontium and europium in $SrAl_2O_4:Eu^{3+}$ films as measured by EDS. For different concentrations of europium in the deposition solution.

Atomic % ± 0.5%				
At%	**O**	**Al**	**Sr**	**Eu**
Eu 0	56.0	31.0	13.0	0
Eu 2	58.0	29.0	12.7	0.3
Eu 4	56.0	27.0	15.0	2.0
Eu 6	56.0	28.0	13.5	2.5
Eu 8	56.0	26.0	14.0	4.0
Eu 10	56.0	27.0	13.0	4.0

while those for the films doped with terbium and europium are larger, about 2–4 μm; undoubtedly the presence of RE ions into the $SrAl_2O_4$ host lattice promotes the growing of these particles.

Fig. 3 shows the XPS survey spectra for a) $SrAl_2O_4:Tb^{3+}$ (8 at%), b) $SrAl_2O_4:Eu^{3+}$ (6 at%) and c) $SrAl_2O_4$ films. Curve 3c shows the presence of the elements Strontium (Sr 3d at 134 eV), Aluminum (Al 2p at 74 eV) and Oxygen (O 1s at 530 eV); the other curves (3a and 3b) exhibit also the presence of terbium and europium, respectively.

In an enlargement of Fig. 3b it is possible to observe that some fraction of Eu^{3+} is reduced to Eu^{2+} (see Fig. 4). The percentages of Eu^{3+} and Eu^{2+} are 65.5% and 34.5%, respectively. Also, it is found that the binding energies for Eu^{2+} (Eu 3d) are centered at 1123 and 1153 eV and for Eu^{3+} (Eu 3d) are centered at 1142 and 1165 eV, in the proportions already mentioned.

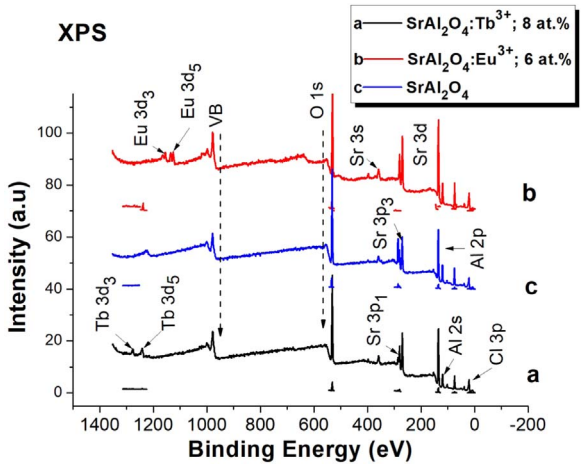

Fig. 3. XPS survey spectra of $SrAl_2O_4$, $SrAl_2O_4:Tb^{3+}$ (8 at%), and $SrAl_2O_4:Eu^{3+}$ (6 at%) films, showing the binding energy (eV) of the elements present in the samples.

Table 3 shows the percentages of Eu^{3+} and Eu^{2+} in the $SrAl_2O_4$:Eu films, for the different doping concentrations studied in this work. It can be seen that the concentrations for Eu^{3+} are higher than for Eu^{2+} in all cases.

Fig. 5 shows the PL excitation spectrum for the $SrAl_2O_4:Tb^{3+}$ (8 at

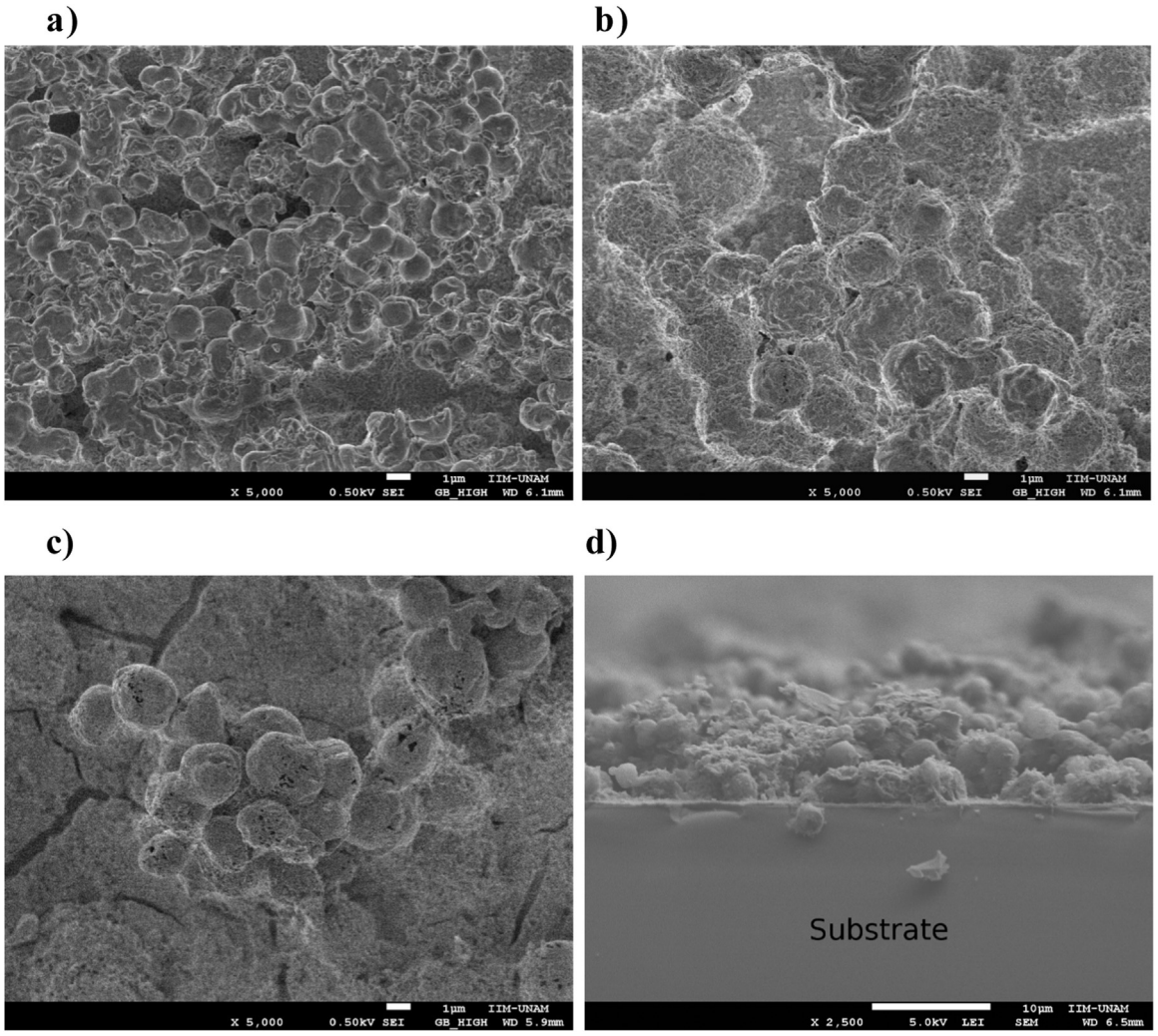

Fig. 2. SEM micrographs of a) $SrAl_2O_4$, b) $SrAl_2O_4:Tb^{3+}$ (8 at%) and c) $SrAl_2O_4:Eu^{3+}$ (6 at%) films; d) cross section of $SrAl_2O_4:Tb^{3+}$ film.

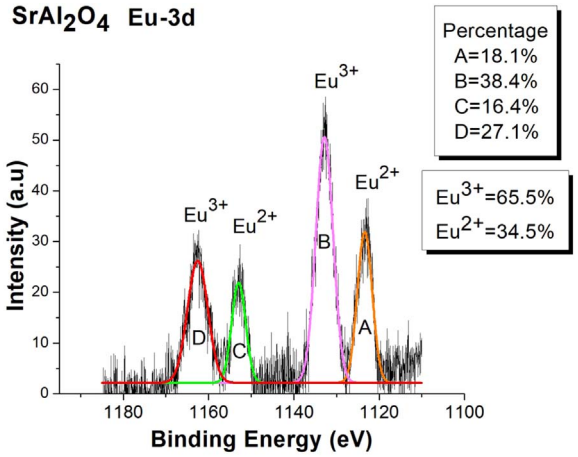

Fig. 4. XPS enlargement of the survey spectra of Eu-3d, showing the binding energy (eV) and the percentages of Eu^{+3} (65.5%)–Eu^{2+} (34.5%).

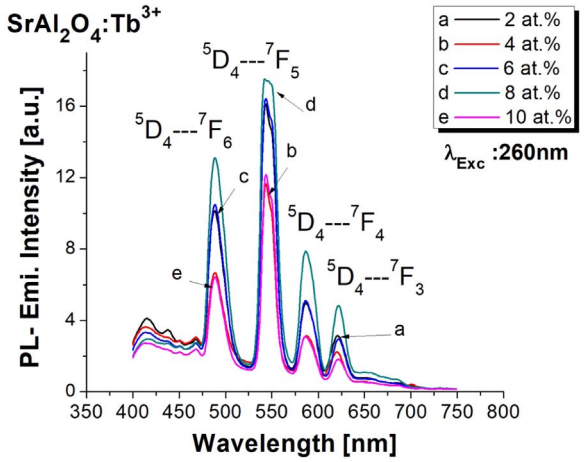

Fig. 6. PL emission spectra for $SrAl_2O_4$:Tb^{3+} films. As a function of the doping concentration, the excitation wavelength was 260 nm.

Table 3
The percentages of Eu^{3+} and Eu^{2+} for the $SrAl_2O_4$:Eu films with different europium doping concentration in the spraying solution.

Percentages		
	% Eu^{3+}	% Eu^{2+}
2 at%	54.5	45.5
4 at%	62.9	37.1
6 at%	63.5	36.5
8 at%	65.5	34.5
10 at%	72.8	27.2

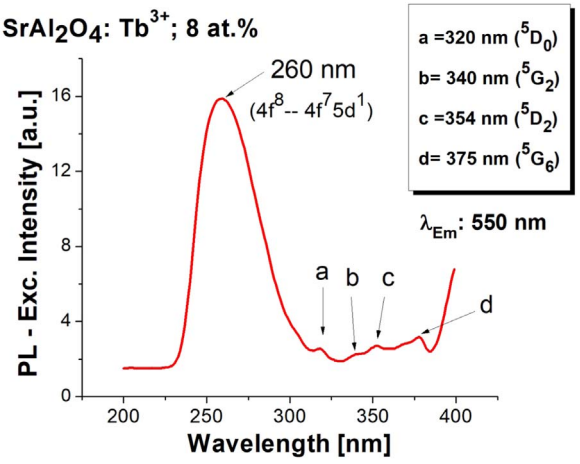

Fig. 5. PL excitation spectrum of $SrAl_2O_4$:Tb^{3+} (8 at%) films. The excitation spectrum was recorded monitoring the emission band at 550 nm.

%) films, which was monitored with an emission wavelength at 550 nm. It is possible to observe bands centered at the following wavelengths λ = 260 nm, 320 nm, 340 nm, 354 nm and 375 nm. The wide and most intense band centered at 260 nm is attributed to the transition $4f^8$–$4f^7 5d^1$ of Tb^{3+} ions [39,40]. The other bands at 320 nm, 340 nm, 354 nm and 375 nm correspond to the transitions in the energy levels of Tb^{3+} ions, which are 320 nm ($^5D_0$), 340 nm ($^5G_2$), 354 nm ($^5D_2$) and 375 nm ($^5G_6$). In this work, the wavelength of 260 nm was used to excite the $SrAl_2O_4$:Tb^{3+} films.

Fig. 6 displays the PL emission spectra for $SrAl_2O_4$:Tb^{3+} films resulting from variations in the terbium doping concentration (2, 4, 6, 8 and 10 at%). The excitation wavelength was 260 nm. In all curves, bands centered at 490 nm, 550 nm, 587 nm and 624 nm are observed, which correspond to the transitions $^5D_4 \rightarrow {}^7F_6$, $^5D_4 \rightarrow {}^7F_5$, $^5D_4 \rightarrow {}^7F_4$ and $^5D_4 \rightarrow {}^7F_3$, respectively. Here it is possible to see that optimal terbium concentration for the best emission intensity in the $SrAl_2O_4$ host lattice is 8 at% in the precursor solution (3.0 as measured by EDS, see Table 1). Higher concentrations of terbium (> 8 at%) produce a decrease in the PL emission intensity; this is due to an effect known as concentration quenching (CQ). It is well known that an increase in the concentration of an activator ion inside a certain host lattice generates a raise in the emitted radiation intensity; this is due to an increase in the absorption efficiency. But, this conduct only is appreciated with a certain critical concentration of the activator ions; for higher concentrations the luminescent intensity decreases. This effect is well known as (CQ) of the luminescence. The concentration quenching depends on a very efficient energy transfer among the activator ions. Energy transfer is favored when the average distance between the activator ions is shortened. Under an efficient energy transfer the excitation energy travels through a large number of activators before being emitted. All host lattices have a certain concentration of defects that can act as acceptors of the excitation energy. These acceptors can relax to their ground state by multi-phonon emission. In this sense they act as an energy sink or quenching traps which promotes the luminescence CQ. On the other hand, the CQ can also be generated without real migration of the excitation energy among the activator ions. This occurs when the excitation energy is lost from the emitting state by means of a cross relaxation mechanism; this mechanism take place by a resonant energy transfer between two identical adjacent luminescent centers, owing to the specific energy-level structure of these centers. Also, it is significant to reveal that moreover the possibility of energy transfer, a high concentration of activator ions can generate new kinds of luminescent centers, such as clusters of individual activators; those new centers can acquire a different energy level scheme to that of the isolated activators, which originates new absorption and emission bands. This is an alternative mechanism of CQ for the luminescence of the isolated activators [41,42].

Fig. 7 exhibits the behavior of the CL emission spectra for $SrAl_2O_4$:Tb^{3+} films as a function of the doping concentration. The applied electron accelerating voltage was 5 kV. All spectra show bands centered at 490 nm ($^5D_4 \rightarrow {}^7F_6$), 550 nm ($^5D_4 \rightarrow {}^7F_5$), 587 nm ($^5D_4 \rightarrow {}^7F_4$) and 624 nm ($^5D_4 \rightarrow {}^7F_3$) corresponding to the emissions of Tb^{3+} ions; the most intense band is centered at 550 nm (green emission). Again, as in the case of PL, 8 at% of terbium ions is the optimal concentration to achieve the maximum emission intensity.

Fig. 8 presents the behavior of the CL emission spectra for $SrAl_2O_4$:Tb^{3+} (8 at%) films as a function of the applied electron accelerating voltage. Once again, these spectra present emission bands centered at 490 nm, 550 nm, 587 nm and 624 nm, which belong to

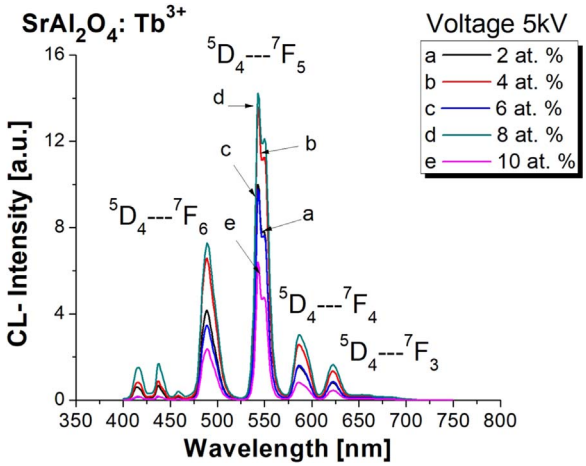

Fig. 7. CL emission spectra of $SrAl_2O_4:Tb^{3+}$ films. As a function of the doping concentration of Tb, the electron accelerating voltage was fixed at 5 kV.

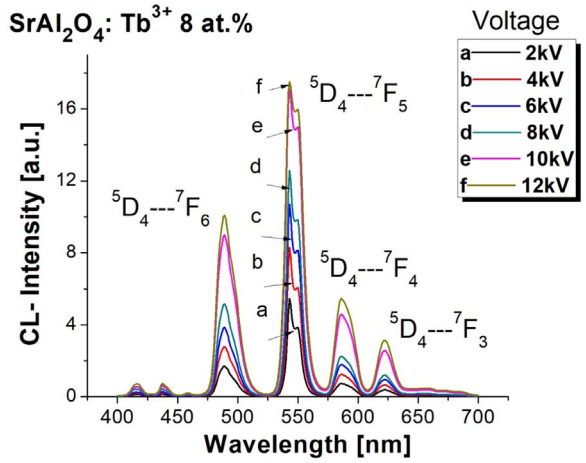

Fig. 8. CL emission spectra for $SrAl_2O_4:Tb^{3+}$ (8 at%) films, with variations in the applied electron accelerating voltages (2, 4, 6, 8, 10 and 12 kV).

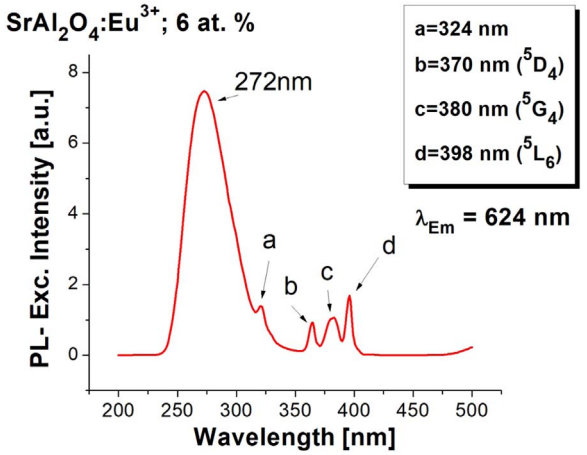

Fig. 9. PL excitation spectrum for $SrAl_2O_4:Eu^{3+}$ (6 at%) films, recorded monitoring the emission at 624 nm.

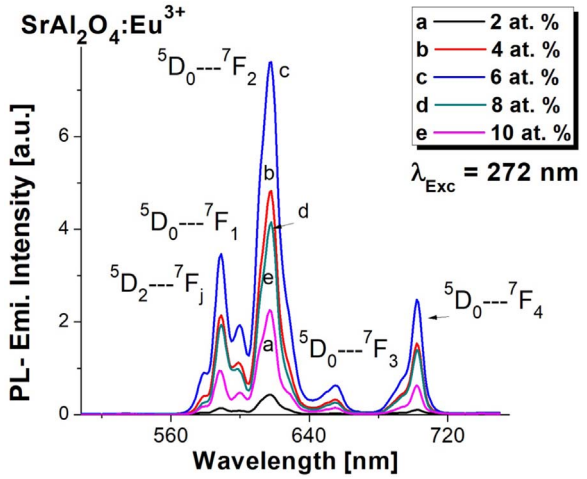

Fig. 10. PL emission spectra for $SrAl_2O_4:Eu^{3+}$ films, as a function of the doping concentration, the excitation wavelength was 272 nm.

electronic transitions in the trivalent terbium ions. In this case, it is observed that as the electron accelerating voltage rises, the CL emission intensity is also increased. As the energy of the incident electrons grows, they penetrate more into the films, this produces a greater amount of excited luminescent centers, consequently a superior quantity of visible photons is generated, in this way an increase in the emission intensity is observed [43].

Fig. 9 displays the excitation spectrum for $SrAl_2O_4:Eu^{3+}$ (6 at%) films. This spectrum presents bands centered at 272 nm, 324 nm, 370 nm, 380 nm and 398 nm, the most intense peak is at $\lambda = 272$ nm, this wide band is attributed to the charge transfer transition from the orbital p of the O^{2-} to f orbital of Eu^{3+} [44]. The small bands at 370 nm, 380 nm and 398 nm correspond to the electronic transitions in Eu^{3+} ions; these transitions go from the ground state of the europium ions to the excited states $^5D_4$, $^5G_4$ and $^5L_6$, respectively. This spectrum was obtained by monitoring the red emission band centered at 624 nm. From this spectrum, $\lambda = 272$ nm was chosen to excite the $SrAl_2O_4:Eu^{3+}$ films.

Fig. 10 exhibits the behavior of the PL emission spectra for $SrAl_2O_4:Eu^{3+}$ films, as a function of the doping concentration; the excitation wavelength was 272 nm. Here, it is possible to observe bands centered at 580 nm, 592 nm, 624 nm, 656 nm and 700 nm, which correspond to the electronic transitions $^5D_2 \rightarrow {}^7F_j$, $^5D_0 \rightarrow {}^7F_1$, $^5D_0 \rightarrow {}^7F_2$, $^5D_0 \rightarrow {}^7F_3$ and $^5D_0 \rightarrow {}^7F_4$, respectively of the Eu^{3+} ions. In this case, it is observed that as the concentration of europium ions increases, the intensity of the emission also increases; however for values greater than 6 at% a decrease in the emission intensity is observed (concentration quenching). This shows that 6 at% of europium ions (in the deposition solution or 2.5 at% as measured by EDS, see Table 2) is the optimal value to reach the maximum PL emission intensity.

Fig. 11 presents the behavior of CL emission spectra for the europium-doped $SrAl_2O_4$ films, with variations in the doping concentration; the electron accelerating voltage was 5 kV. These spectra show bands positioned at 580 nm, 592 nm, 624 nm, 656 nm and 700 nm which correspond to the electronic transitions of the Eu^{3+} ions (curves I, II, III and IV). In addition, there appears a broadband centered at 525 nm, which could be associated with Eu^{2+} ions [32]. Because the Eu^{2+} broadband is the most intense, the CL emissions look yellowish-green and not red like the case of the PL spectra. Also, the most intense CL emission is reached for a concentration of 6 at% of europium ions. A quenching concentration is observed for europium concentration greater than 6 at%. The appearance of the wide band centered on 525 nm and associated with Eu^{2+} ions is completely unexpected. This fact cannot be explained with the information we have so far. It is known that Eu^{3+} ions can be reduced to Eu^{2+} by thermal treatments in a reducing atmosphere [45], in this work the thermal treatments were carried out in a normal atmosphere (air). Therefore, further research is needed to completely elucidate this point.

In Fig. 12 the CL emission spectra for $SrAl_2O_4:Eu^{3+}$ (6 at%) films as a function of the applied electron accelerating voltage are shown. As a

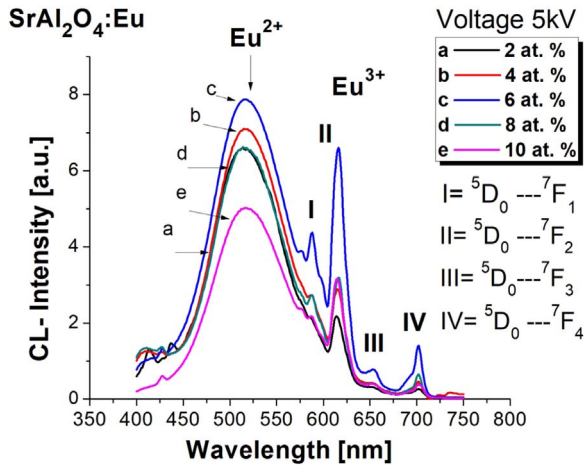

Fig. 11. CL emission spectra for $SrAl_2O_4$:Eu films, as a function of the europium ions concentration, the electron accelerating voltage was 5 kV.

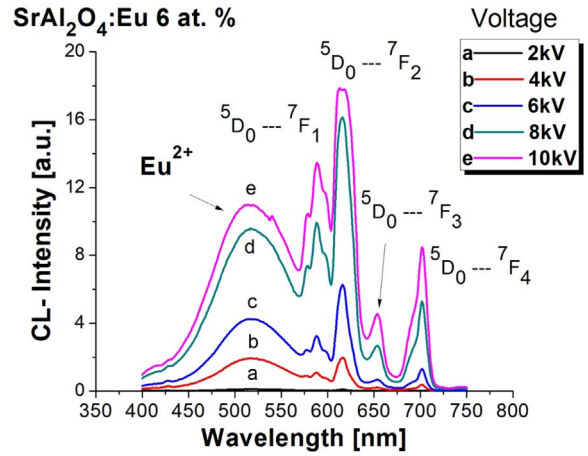

Fig. 12. CL emission spectra for $SrAl_2O_4$:Eu^{3+} (6 at%) films, with variations in the applied electron accelerating voltages (2, 4, 6, 8 and 10 kV).

whole the spectra grow in intensity as the electron accelerating voltage increases; this may be because more energetic electrons excite a larger volume of material and generate more visible light. In addition, the bands belonging to the trivalent europium ions also increase and even become larger than the wide bands centered at 525 nm. Some of these samples appear yellowish as a result of the simultaneous emission of Eu^{3+} ions (red) and Eu^{2+} ions (green). The CL emission is a very complex phenomenon; the interaction between the accelerated electrons and the solid film generates several signals, which include: secondary electrons, backscattered electrons, Auger electrons, X-rays, visible light, etc. Some of them can in turn act as sources of excitation for the various luminescent centers present within the films; although at the moment it is not possible to say which of them excite more efficiently. The experimental results indicates that the electrons with higher energy produce a greater intensity in the bands corresponding to Eu^{3+} ions with respect to that for Eu^{2+} ions.

Fig. 13 displays the CIE chromaticity diagram for CL and PL from $SrAl_2O_4$:Eu^{3+}: Eu^{2+} films. In this diagram it is possible to observe points which represents some colors: yellowish-green (point A), yellow (point B) and red (point C); these three colors come from the same film, but excited by two different methods (CL and PL) and different electron acceleration voltages in the case of CL. The excitation of $SrAl_2O_4$:Eu^{3+}: Eu^{2+} films with low energy electrons in CL, produce a yellowish-green color, but by increasing the electron acceleration voltage up to 10 kV the films emit a yellow color. The above allows color tuning only with electron accelerating voltage variations. If the $SrAl_2O_4$:Eu^{3+}: Eu^{2+}

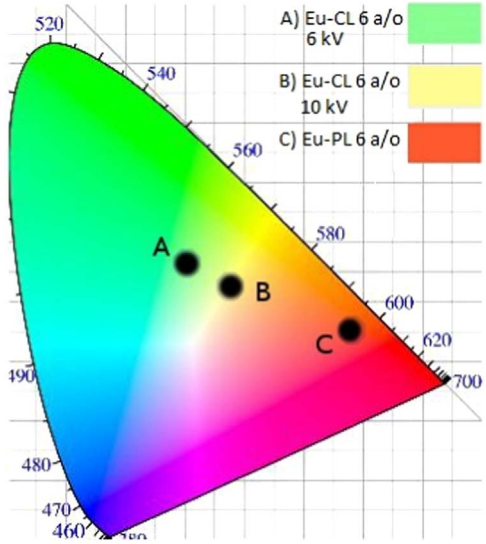

Fig. 13. CIE chromaticity diagram for $SrAl_2O_4$:Eu (6 at%) films, excited by photons (PL) and accelerated electrons (CL). a. (For interpretation of the references to color in this figure, the reader is referred to the web version of this article.)

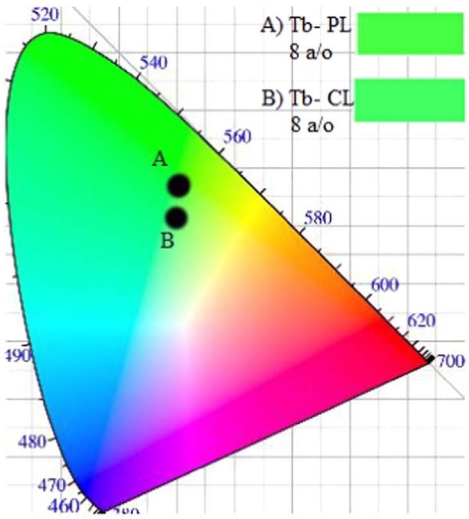

Fig. 14. CIE chromaticity diagram for $SrAl_2O_4$:Tb^{3+} (8 at%) films. The points represent emissions from PL and CL emissions. (For interpretation of the references to color in this figure, the reader is referred to the web version of this article.)

films are excited by ultraviolet photons (PL) the color emission is red.

Fig. 14 shows the CIE chromatic diagram for CL and PL from $SrAl_2O_4$:Tb^{3+} (8 at%) films. The color showed in this diagram is green (A and B), the coordinates of these points in the chromatic diagram are (0.3186, 0.5724), (0.3074, 0.5454), respectively. The changes in the color of the PL and CL emissions probably are due to the excitation with UV photons and accelerated electrons are of different nature.

Fig. 15 displays curves of the luminescence decay for $SrAl_2O_4$:Eu^{3+} (6 at%) and for $SrAl_2O_4$:Tb^{3+} (8 at%) films (Fig. 15a and b). The decay curve for $^5D_4 \rightarrow {}^7F_5$ (550 nm) transition of Tb^{3+} ions can be well fitted into a triple-exponential function as: $I = A + B_1exp(-t/\tau_1) + B_2exp(-t/\tau_2) + B_3exp(-t/\tau_3)$ and the decay curve for $^5D_0 \rightarrow {}^7F_3$ (624 nm) transition of Eu^{3+} ions was fitted into a double-exponential function as: $I = A + B_1exp(-t/\tau_1) + B_2exp(-t/\tau_2)$. In both cases I is the PL intensity and A (background), Bn and τ_n are the fitting parameters, the numerical values of these parameters are listed in Table 4. The average decay times (τ_a) were calculated by the following equation: $\tau_a = [\Sigma B_i(\tau_i)^2]/[\Sigma B_i(\tau_i)]$, the average decay time values were 2.7 ms for $SrAl_2O_4$:Tb^{3+} films and 1.9 ms for $SrAl_2O_4$:Eu^{3+} films; these average decay times are

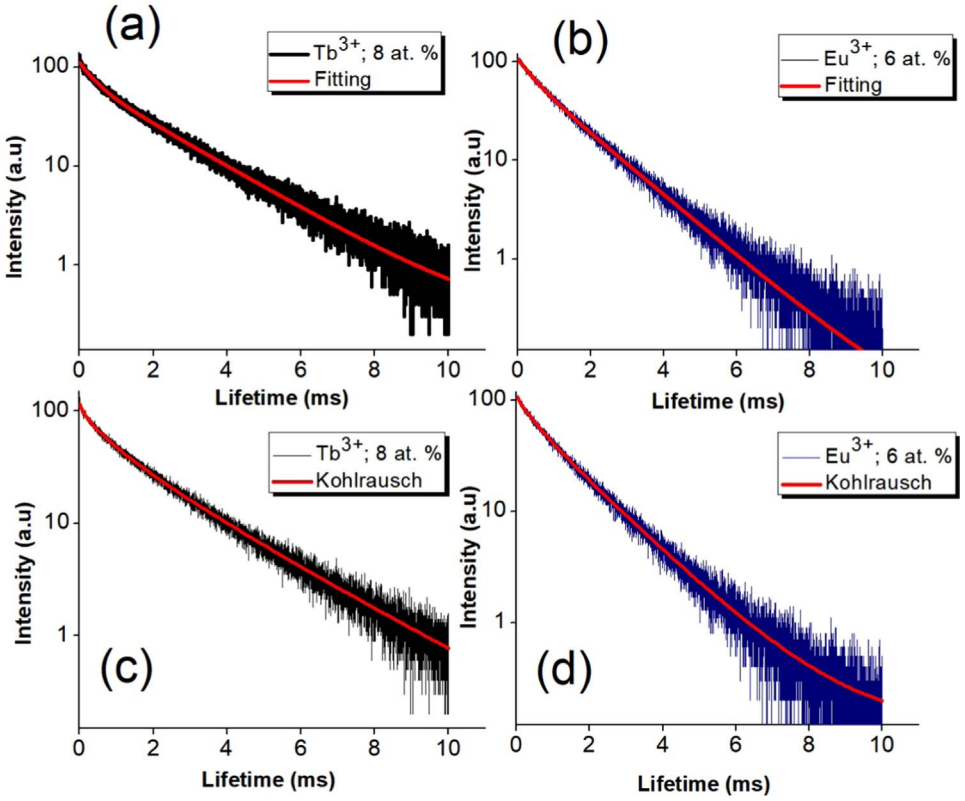

Fig. 15. Curves and fittings of decay time for a) $SrAl_2O_4:Tb^{3+}$ (8 at%) and b) $SrAl_2O_4:Eu^{3+}$ (6 at%), obtained by the multi-exponential approach. Curves and fittings of decay time for stretched exponential model for c) $SrAl_2O_4:Tb^{3+}$ (8 at%) and d) $SrAl_2O_4:Eu^{3+}$ (6 at%).

comparable to those obtained in other contributions [44].

However, with the present information it is difficult to give an explanation, from the physical point of view, of the adjustment of the decay curve with three exponentials. Frequently the excited luminescent activators are in an inhomogeneous environment and quenching processes and other environmental influences (including energy transfer) can lead to complex luminescence decays or multi-exponential decay behavior. Another approach to solve the multi-exponential behavior of PL decay is through the Kohlrausch function (or stretched exponential model) [46]; this Kohlrausch function is known to describe well the luminescence decay of several classes of systems such as ordered and disordered inorganic solids and of semiconductor nanoclusters [47], and is expressed mathematically as:

$$\Phi(t) = \Phi(0)\exp[-(t/\tau)^{\beta}], \text{ were } 0 < \beta < 1.$$

In the simplest situation, where the separation between the activator ion and the interaction sites is regularly distributed, the total decay function is calculated by the integration of the differential equation that explains the time evolution of the excited state and the summing-up over all sites [46], i. e.

$$\Phi(t) = \Phi(0)\exp[-(1 + c)t/\tau - a(t/\tau)^{1/2}],$$

where **a** represents the interaction parameter between the activator ions and host lattice assuming a dipole-dipole interaction and **c** is the quenching parameter.

Curves of the luminescence decay for $SrAl_2O_4:Tb^{3+}$ (8 at%) and $SrAl_2O_4:Eu^{3+}$ (6 at%) films were obtained by the stretched exponential model and are presented in Fig. 15c and d, respectively. The numerical values of the fittings for time decays, by means of this model, are also presented in Table 4, where the **c** parameter is fixed to zero. The values of the PL decay times for Tb^{3+} and Eu^{3+} ions, obtained with the Kohlrausch model, are similar to the time decay averages presented in Fig. 15a and b (see Table 4) considering a multi-exponential behavior. In the case of $SrAl_2O_4:Tb^{3+}$ films (τ = 3.4 ms, Kohlrausch model) the result indicates a strong interaction between the Tb^{3+} ions and the host lattice ions. In general, the single non-exponential decay is due to inhomogeneities in the vicinity of the Tb^{3+} ions, these may be probably Tb^{3+} ion clusters or separate Tb^{3+} ions not homogeneously distributed [42]. Also, probably, the incorporation of Tb^{3+} ions in different spectroscopic sites gives rise to changes in the decay times, causing the need to fit the curve with several exponentials.

For the case of $SrAl_2O_4:Eu^{3+}$ films the decay time (τ = 1.7 ms) obtained by Kohlrausch function, is very similar to that obtained by fitting with two exponentials (τ = 1.9 ms). In the present case, the parameter **a** that indicates the interaction of Eu^{3+} ions with the host lattice is lower as compared to that for the Tb^{3+} ions (see Table 4). Here

Table 4
Fitting parameters of the decay time for $SrAl_2O_4:Tb^{3+}$ (8 at%), $SrAl_2O_4:Eu^{3+}$ (6 at%) films obtained by multi-exponential approach, and Kohlrausch model for $SrAl_2O_4:Tb^{3+}$ (8 at%) and $SrAl_2O_4:Eu^{3+}$ (6 at%) films.

$SrAl_2O_4:Tb^{3+}$		$SrAl_2O_4:Eu^{3+}$		$SrAl_2O_4:Tb^{3+}$ Kohlrausch model		$SrAl_2O_4:Eu^{3+}$ Kohlrausch model	
Coefficient	Decay Times (ms)	Coefficient	Decay Times (ms)	Coefficient	Value	Coefficient	Value
A = 1.9	τ_1 = 0.04	A = 0.1	τ_1 = 0.43	a	1.2	a	0.6
X^2 = 1.3	τ_2 = 0.59	X^2 = 1.1	τ_2 = 1.43	c	0	c	0
B_1 = 531.4	τ_3 = 2.11	B_1 = 303.1		Φ(0)	1.3	Φ(0)	1.2
B_2 = 663.1		B_2 = 762.2		X^2 =	0.996	X^2 =	0.997
B_3 = 320.9	τ_a = 2.7		τ_a = 1.9	τ = 3.4 ms		τ = 1.7 ms	

it is important to note that these films show the simultaneous presence of Eu^{2+} and Eu^{3+} ions as indicated by the XPS results. Probably the fitting with two exponentials is associated with the presence of these two types of ions.

4. Conclusions

$SrAl_2O_4$, $SrAl_2O_4$:Tb^{3+} and $SrAl_2O_4$:Eu^{3+} films were successfully deposited by the ultrasonic spray pyrolysis method. The SEM micrographs showed rough surfaces for all films formed of clusters of spheroid particles of 1.5–4 μm in diameter. Films deposited at 550 °C were non-crystalline; it was necessary to anneal these samples at 800 °C to obtain the monoclinic phase of $SrAl_2O_4$ with the spatial group *2P1*. The grain sizes (estimated by the Scherrer formula) for $SrAl_2O_4$, $SrAl_2O_4$:Tb^{3+} and $SrAl_2O_4$:Eu^{3+} films were 24.4, 26.39 and 27.82 nm, respectively. EDS measurements showed an stoichiometry close to the ideal for $SrAl_2O_4$. The PL emission spectra for $SrAl_2O_4$:Tb^{3+} films exhibited the typical bands corresponding to the electronic transitions of the Tb^{3+} ions; the green band centered at 550 nm ($^5D_4 \rightarrow {}^7F_5$) was the most intense. It was demonstrated that an 8 at% of terbium ions (in the deposition solution or 3 at% inside the films as measured by EDS) is the optimum value that provides the maximum PL and CL emission intensity. In addition, it was observed that as the electron accelerating voltage increased, the intensity of the CL emission also increased. PL emission spectra for $SrAl_2O_4$:Eu^{3+} films showed bands corresponding to the electronic transitions of europium ions. The band at 624 nm was the highest intensity; in this case, the concentration quenching was achieved for values (of the europium ions) greater than 6 at% (in the precursor solution or 2.5 at% as measured by EDS). The averaged decay time for $SrAl_2O_4$:Tb^{3+} (8 at%) films were 2.7 ms and 1.9 ms for $SrAl_2O_4$:Eu^{3+} (6 at%) films. The decay times obtained by the stretched exponential model were 3.4 ms and 1.7 ms, respectively. The CL emission spectra for europium-doped $SrAl_2O_4$ films exhibited the emission bands typical of Eu^{3+} ions and, in addition, a broadband centered at 525 nm (green color) which was associated with the Eu^{2+} ions. The intensity of this band depends on the values of applied electron accelerating voltage. Thus, it is possible to obtain various colors (tuning) from $SrAl_2O_4$:Eu^{3+}:Eu^{2+} films varying the energy of the incident electrons. The presence of Eu^{3+} and Eu^{2+} ions was confirmed by XPS measurements. It is remarkable the reduction of Eu^{3+} to Eu^{2+} without using an intentional reducing atmosphere during the heat treatments. CIE chromaticity diagrams exhibited the emission in various colors: green from $SrAl_2O_4$:Tb^{3+} films, red, green and yellow from $SrAl_2O_4$:Eu^{3+} and $SrAl_2O_4$:Eu^{3+}:Eu^{2+} films, respectively.

Acknowledgments

The authors R. M. Calderón-Olvera and E. A. Albanés-Ojeda would like to thank to CONACYT (scholarships No.: 487111 and No.: 486933, respectively), also to Adriana Tejeda for XRD measurements, Omar Novelo for SEM and EDS measurements, Lazaro Huerta for XPS measurements, Vicente Vargas, Raúl Reyes and Carlos Flores for their technical support.

References

[1] G. Blasse, A. Bril, Fluorescence of Eu^{2+} activated alkaline-earth aluminates, Philips Res. Rep. 23 (1968) 201–206.
[2] W.L. Wanmaker, J.W. terVrugt, Luminescence of calcium orthophosphates activated with divalent europium, Philips Res. Rep. 22 (1968) 362–366.
[3] F. Clabau, X. Rocquefelte, S. Jobic, P. Deniard, M.-H. Whangbo, A. Garcia, T. Le Mercier, Mechanism of phosphorescence appropriate for the long-lasting phosphors Eu^{2+}-doped $SrAl_2O_4$ with codopants Dy^{3+} and B^{3+}, Chem. Mater. 17 (2005) 3904–3912.
[4] T. Matsuzawa, Y. Aoki, N. Takeuchi, Y. Murayama, A new long phosphorescent phosphor with high brightness, SrAl2O4:Eu^{2+}, Dy^{3+}, J. Electrochem. Soc. 143 (1996) 2670–2673.
[5] B.G. Zhai, Q.L. Ma, Y.M. Huang, Combustion synthesis and luminescent properties of Eu^{3+} and Dy^{3+} co-doped amorphous $SrAl_2O_4$, Key Eng. Mater. 538 (2013) 58–62.
[6] K. Van den Eeckhout, P.F. Smet, D. Poelman, Persistent luminescence in Eu^{2+}-doped compounds: a review, Materials 3 (2010) 2536–2566.
[7] Z. Fu, S. Zhou, T. Pan, S. Zhang, Band structure calculations on the monoclinic bulk and nano-$SrAl_2O_4$ crystals, J. Solid State Chem. 178 (2005) 230–233.
[8] B.M. Mothudi, O.M. Ntwaeaborwa, A. Kumar, K. Sohn, H.C. Swart, Phosphorescent and thermoluminescent properties of SrAl2O4:Eu^{2+}, Dy^{3+} phosphors prepared by solid state reaction method, Physica B: Condens. Matter 407 (2012) 1679–1682.
[9] R. Meléndrez, O. Arellano-Tánori, M. Pedroza-Montero, W.M. Yen, M. Barboza-Flores, Temperature dependence of persistent luminescence in β-irradiated $SrAl_2O_4$:Eu^{2+}, Dy^{3+} phosphor, J. Lumin. 129 (2009) 679–685.
[10] B.M. Mothudi, M.A. Lephoto, O.M. Ntwaeaborwa, J.R. Botha, H.C. Swart, Thermoluminescent and structural properties of BaAl2O4:Eu^{2+}, Nd^{3+}, Gd^{3+} phosphors prepared by combustion method, Physica B 407 (2012) 1620–1623.
[11] K. Kato, I. Tsutai, T. Kamimura, F. Kaneko, K. Shinbo, M. Ohta, T. Kawakami, Thermoluminescence properties of $SrAl_2O_4$:Eu sputtered films with long phosphorescence, J. Lumin. 82 (1999) 213–220.
[12] A. Ebrahimzade, M.R.M. Mojtahedi, R.S. Rahbar, Preparation and characterisation of luminous polypropylene/phosphor strontium aluminate nanocomposite fibres with enhanced dyeability, Plast. Rubber Compos. 45 (8) (2016) 368–373.
[13] X. Ch. Shi, X. Hou, M. Li, Ge, Preparation and characterization of persistent luminescence of regenerated cellulose fiber, J. Mater. Sci.: Mater. Electron. 28 (2016) 1015–1021.
[14] Y. Zhu1, Z. Pang, J. Wang, M. Ge, A. Ju, Research on the afterglow properties of red-emitting phosphor: $SrAl_2O_4$:Eu^{2+}, Dy^{3+}/light conversion agent for red luminous fiber, J. Mater. Sci.: Mater. Electron. 27 (2016) 7554–7559.
[15] J. Yang, B. Yanmei, G. Mingqiao, Preparation and luminescence properties of a white emitting long afterglow luminous fiber based on FRET, J. Rare Earths 34 (4) (2016) 374–380.
[16] V. Sharma, A. Das, V. Kumar, Eu^{2+}, Dy^{3+} codoped $SrAl_2O_4$ nanocrystalline phosphor for latent fingerprint detection in forensic applications, Mater. Res. Express 3 (2016) (DOI: 015004).
[17] L. Liu, Z. Zhang, L. Zhang, Y. Zhai, The effectiveness of strong afterglow phosphor powder in the detection of fingermarks, Forensic Sci. Int. 183 (2009) 45–49.
[18] A. Sepahvandi, M. Eskandari, F. Moztarzadeh, Fabrication and characterization of SrAl2O4:Eu^{2+} Dy^{3+}/CS-PCL electrospun nanocomposite scaffold for retinal tissue regeneration, Mater. Sci. Eng. C 66 (2016) 306–314.
[19] I.P. Sahu, Enhance luminescence by introducing alkali metal ions (R+ = Li+, Na+ and K+) in SrAl2O4:Eu^{3+} phosphor by solid-state reaction method, Radiat. Eff. Defects Solids 171 (2016) 511–527.
[20] B. Li, J. Zhang, M. Zhang, Y. Long, X. He, Effects of $SrCl_2$ as a flux on the structural and luminescent properties of $SrAl_2O_4$:Eu^{2+}, Dy^{3+} phosphors for AC-LEDs, J. Alloy. Compd. 651 (2015) 497–502.
[21] G. Blasse, B.C. Grabmaier, Luminescent Materials, Springer Verlag, Berlin Heidelberg, 1994 (Cap. 2).
[22] H.C. Swart, J.J. Terblans, O.M. Ntwaeaborwa, R.E. Kroon, B.M. Mothudi, PL and CL degradation and characteristics of SrAl2O4:Eu^{2+}, Dy^{3+} phosphors, Physica B: Condens. Matter 407 (2012), pp. 1664–1667.
[23] Y.M. Huang, Q. Ma, Long afterglow of trivalent dysprosium doped strontium aluminate, J. Lumin. 160 (2015) 271–275.
[24] H. Du, W. Shan, L. Wang, D. Xu, H. Yin, Y. Chen, D. Guo, Optimization and complexing agent-assisted synthesis of green $SrAl_2O_4$:Eu^{2+}, Dy^{3+} phosphors through sol–gel process, J. Lumin. 176 (2016) 272–277.
[25] B. Zhai, L. Yang, Q. Ma, X. Liu, Y.M. Huang, Mechanism of the prolongation of the green afterglow of $SrAl_2O_4$:Dy^{3+} caused by the use of H_3BO_3 flux, J. Lumin. 181 (2017) 78–87.
[26] D.S. Kshatri, A. Khare, Comparative study of optical and structural properties of micro- and nanocrystalline $SrAl_2O_4$:Eu^{2+}, Dy^{3+} phosphors, J. Lumin. 155 (2014) 257–268.
[27] J. Zhang, M. Ge, Effecting factors of the emission spectral characteristics of rare-earth strontium aluminate for anti-counterfeiting application, J. Lumin. 131 (2011) 1765–1769.
[28] S.Y. Kaya, E. Karacaoglu, B. Karasu, Effect of Al/Sr ratio on the luminescence properties of SrAl2O4:Eu^{2+}, Dy^{3+} phosphors, Ceram. Int. 38 (2012) 3701–3706.
[29] C.R. García, L.A. Diaz-Torres, J. Oliva, M.T. Romero, P. Salas, Photocatalytic activity and optical properties of blue persistent phosphors under UV and solar irradiation, Int. J. Photoenergy 2016 (2016) (ID 1303247).
[30] D.S. Kshatri, A. Khare, P. Jha, Effects of Dy concentration on luminescent properties of $SrAl_2O_4$: Eu phosphors, Optik 124 (2013) 2974–2978.
[31] P.T. Ji, X.Y. Chen, Y.Q. Wu, Encapsulating MAl2O4:Eu^{2+}, Dy^{3+} (M = Sr, Ca, Ba) phosphors with triethanolamine to enhance water resistance, Appl. Surf. Sci. 258 (2011) 1888–1893.
[32] H. Yamada, X. Fu, Ch Xu, Triboluminescence of SrAl2O4:Eu film with strong adhesion fabricated by a combination of RF magnetron sputtering and post-annealing treatment, Key Eng. Mater. 368–372 (2008) 1362–1365.
[33] S.F. Yan, K.G. Miao, Luminescent property of Al_2O_3:Ce^{3+} thin films, Appl. Mech. Mater. 130–134 (2012) 23–26.
[34] H. Suematsu, M. Sengiku, K. Kato, M. Mitome, K. Kimoto, Y. Matsui, W. Jiang, K. Yatsui, Photoluminescence properties of crystallized strontium aluminate thin films prepared by ion-beam evaporation, Thin Solid Films 407 (2002) 136–138.
[35] H.C. Swart, E. Coetsee, J.J. Terblans, O.M. Ntwaeaborwa, P.D. Nsimama, F.B. Dejene, J.J. Dolo, Cathodoluminescence degradation of PLD thin films, Appl. Phys. A 101 (2010) 633–638.
[36] A.H. Wako, F.B. Dejene, H.C. Swart, Structural and luminescence properties of SrAl2O4:Eu^{2+}, Dy^{3+}, Nd^{3+} phosphor thin films grown by pulsed laser deposition,

Physica B 480 (2016) 116–124.
[37] H.C. Swart, O.M. Ntwaeaborwa, P.D. Nsimama, J.J. Terblans, Surface characterization and luminescent properties of SrAl2O4:Eu^{2+}, Dy^{3+} nano thin films, Physica B 407 (2012) 1660–1663.
[38] P.D. Nsimama, O.M. Ntwaeaborwa, H.C. Swart, Auger electron/X-ray photoelectron and cathodoluminescent spectroscopic studies of pulsed laser ablated SrAl2O4:Eu^{2+}, Dy^{3+} thin films, Appl. Surf. Sci. 257 (2010) 512–517.
[39] D. Yuan, Z. Gao, Z. Jian, J. Shu, Y. Li, X. Tao, Growth, polarized Raman and fluorescence properties of $TbCa_4O(BO_3)_3$ single crystal, Opt. Mater. 42 (2015) 435–440.
[40] Z. Xu, Y. Li, Z. Liu, D. Wang, UV and X-ray excited luminescence of Tb^{3+}-doped $ZnGa_2O_4$ phosphors, J. Alloy. Compd. 391 (2005) 202–205.
[41] J. García Solé, L.E. Bausá, D. Jaque, An Introduction to the Optical Spectroscopy of Inorganic Solids, John Wiley & Sons, Ltd., Chichester, UK, 2005.
[42] G. Pucker, S. Parolin, E. Moser, M. Montagna, M. Ferrari, L. Del Longo, Raman and luminescence studies of Tb3+ doped monolithic silica xerogels, Spectrochim. Acta Part A 54 (1998) 2133–2142.
[43] A. Báez-Rodríguez, O. Álvarez-Fregoso, M. García-Hipólito, J. Guzmán-Mendoza, C. Falcony, Luminescent properties of ZrO_2:Dy^{3+} and ZrO_2:Dy^{3+} +Li^{+} films synthesized by an ultrasonic spray pyrolysis technique, Ceram. Int. 41 (2015) 7197–7206.
[44] J.C. Guzmán-Olguín, E. Montes, J. Guzmán-Mendoza, A. Báez-Rodríguez, L. Zamora-Peredo, M. García-Hipólito, O. Álvarez-Fregoso, I. Martínez-Merlín, C. Falcony, Tunable white light emission from hafnium oxide films co-doped with trivalent terbium and europium ions deposited by Pyrosol technique, Phys. Status Solidi A (2017) 1700269.
[45] C. LeLuyer, M. Villanueva-Ibañez, A. Pillonnet, C. Dujardin, HfO2: X (X = Eu^{3+}, Ce^{3+}, Y^{3+}) Sol gel powders for ultradense scintillating materials, J. Phys. Chem. A 112 (2008) 10152–10155.
[46] G.C. Righini, M. Ferrari, Photoluminescence of rare-earth–doped glasses, Riv. Nuovo Cim. 28 (2005) 12.
[47] M.N. Berberan-Santos, E.N. Bodunov, B. Valeur, Mathematical functions for the analysis of luminescence decays with underlying distributions 1. Kohlrausch decay function (stretched exponential), Chem. Phys. 315 (2005) 171–182.